arXiv:1611.03366v1 [math.DS] 10 Nov 2016

Reconstructing directed and weighted topologies of phase-locked oscillator networks

Francesco Alderisio[†] , Gianfranco Fiore[†] & Mario di Bernardo[†‡] *

The formalism of complex networks is extensively employed to describe the dynamics of interacting agents in several applications. The features of the connections among the nodes in a network are not always provided beforehand, hence the problem of appropriately inferring them often arises. Here, we present a method to reconstruct directed and weighted topologies (REDRAW) of networks of heterogeneous phase-locked nonlinear oscillators. We ultimately plan on using REDRAW to infer the interaction structure in human ensembles engaged in coordination tasks, and give insights into the overall behavior.

[†]Department of Engineering Mathematics, Merchant Venturers Building, University of Bristol, Woodland Road, Clifton, Bristol BS8 1UB, United Kingdom (enmdb@bristol.ac.uk)

[‡]Department of Electrical Engineering and Information Technology, University of Naples Federico II, Via Claudio 21, 80125 Naples, Italy (mario.dibernardo@unina.it)

1 Introduction

The study of complex networks has been a subject of great interest [1, 2, 3, 4]. Indeed, networks provide a rigorous formalism to describe phenomena involving populations of interacting agents in fields as diverse as Physics, Engineering, Biology, Chemistry, Social Science and the Internet [5, 6, 7, 8].

Even though the topology of the interactions among the nodes is often provided, there might be cases in which there is no *a-priori* knowledge of the network structure. Instead, the topology of the interconnections among the nodes has to be reconstructed (or reverse-engineered) from data. Specifically, given a set of simultaneously recorded time series, it is important to identify the information structure characterized by hidden dependencies between the components of a complex dynamical system [9]. In particular, it may be required to identify causal dependencies among the nodes or quantify the flow of information across a specific network. Such flow can be *unidirectional* (the behavior of node/agent A affects that of node/agent B, but not vice versa) or *bidirectional* (the behavior of each of the two nodes/agents depends on that of the other). Moreover, the strength by which the agents influence each other might be different; the information flow in this case is therefore said to be *weighted*. Knowing the topology of the interactions among the agents in a network would allow for a better understanding of their behavior in order to analyze it and predict it, design networks with pre-described functions, and potentially control them [10, 11].

The problem of inferring the existence and direction of links among nodes in a network from a given data-set is a reverse engineering task often referred to as *network reconstruction* or *network inference*. It is of crucial importance to determine which of the inferred connections correspond to links existing in the real interaction structure (*true positives*), and which instead represent only functional connectivities between nodes (*false positives*) [12]. This problem arises in several contexts, e.g., reconstructing functional activation/repression links in gene regulatory networks [13, 14, 15] or causal relationships in stochastic processes [16], understanding the structure of social interactions in a group from communication data [17, 18, 19], and inferring functional relationships between areas in the brain from EEG data [20] or in physiological systems [21]. However, reviews of network inference methods have found large discrepancies among the results of different algorithms [22, 23].

A notable case is that of networks of nodes whose dynamics is oscillatory (e.g., neurones, cellular cycles, synthetic biological oscillators, groups of walking autonomous robots). For these networks, methods for reconstructing their structure from data on their dynamics have been proposed. Examples include the work in [24], dealing with the problem of inferring directed and weighted topologies, as well as that in [25], investigating community detection in undirected and unweighted networks of Kuramoto oscillators [26], and those in [12, 27], tackling the reconstruction of directed and unweighted topologies of small networks of coupled limit cycle oscillators. In these works, none of the inferred connections are removed, or if they are, no formal method is presented on how to choose the thresholds according to which false positive links are to be cut-off.

Here, we present REDRAW (REconstruction of DiRected And Weighted topologies) as a significant extension of the methodology firstly proposed in [25], originally conceived to only detect communities in undirected and unweighted networks of Kuramoto oscillators, widely used to describe synchronization phenomena within populations of interacting agents [28, 29]. We show that REDRAW allows to effectively infer directed and weighted links among a group of coupled oscillators, and present an algorithm that allows to set the cut-off thresholds for removing false positives. We validate the method on a number of representative examples, including a set of real-world networks obtained from [30, 31, 32, 33, 34].

2 Materials and Methods

The mathematical model used to validate REDRAW is a network of n nonuniform Kuramoto oscillators [35, 36], described by

$$\dot{\theta_i} = \omega_i + \frac{c}{n}\sum_{j=1}^{n} a_{ij}\sin(\theta_j - \theta_i - \phi_{ij}),\ i = 1, 2, \ldots, n \tag{1}$$

where $\theta_i \in [-\pi, \pi]$ represents the phase of the ith oscillator, $\omega_i > 0$ its natural frequency, $c > 0$ the global coupling strength among all nodes in the network, and a_{ij} the local influence that node j has on node i. For directed and weighted topologies, in general $a_{ij} \neq a_{ji}$ with $a_{ij} \geq 0\ \forall i, j$. Moreover, the phase shift

$$\phi_{ij} := \begin{cases} \frac{\phi}{a_{ij}}, & aij > 0 \\ 0, & a_{ij} = 0 \end{cases} \tag{2}$$

represents how much node i lags behind node j, with $\phi \in [0, \frac{\pi}{2}]$. Note that the higher the influence a_{ij} that node j has on node i, the lower the phase shift ϕ_{ij} (i.e., the less node i lags behind node j).

We start from a data-set consisting of n time series of duration $T > 0$, one for each of the n oscillators in the network of interest, and assume that K experiments are available for a total of $K \times n$ time series of length

T. The proposed method aims at inferring the topology of the interactions among the nodes by estimating the influence that each agent in the network has on the others, provided *phase-locking* is achieved by the oscillators [37].

REDRAW is a method consisting in a sequence of six steps: first the relative phases among all the nodes are evaluated and parameters representing their respective correlation are derived from them (*Step 1–Step 4*), then two filtering steps (*Step 5* and *Step 6*) are carried out to remove possible false positives in the interactions among the nodes. More specifically:

Step 1. The relative phase $\Delta\theta_{ij,k}(t) = \theta_{i,k}(t) - \theta_{j,k}(t)$, $\forall k = 1, \ldots, K$ with $t \in [0, T]$ is evaluated, where negative values of $\Delta\theta_{ij,k}(t)$ indicate that node i lags behind node j at time instant t of the kth experiment.

Step 2. The parameter $\zeta_{ij,k}(t)$ defined as:

$$\zeta_{ij,k}(t) := \begin{cases} \frac{1+\cos[\Delta\theta_{ij,k}(t)]}{2}, & \Delta\theta_{ij,k}(t) \leq 0 \\ 0, & \Delta\theta_{ij,k}(t) > 0 \end{cases} \tag{3}$$

is calculated for all the possible pairs of nodes in the network. Note that $\zeta_{ij,k}(t) \neq \zeta_{ji,k}(t)$ and that $\zeta_{ij,k}(t) \in [0, 1]$, where $\zeta_{ij,k}(t) = 1$ represents the maximum level of influence that node j has on node i. On the other hand, when $\Delta\theta_{ij,k}(t) > 0$, agent j lags behind agent i, hence the influence that the former has on the latter is assumed to be negligible and set to 0.

Step 3. The average value over time of the parameter defined in Eq. (3) is evaluated as:

$$\rho_{ij,k} := \frac{1}{T} \int_0^T \zeta_{ij,k}(t)\, dt \tag{4}$$

where T is the duration of each time series.

Step 4. The link representative of the overall influence that node j has on node i is inferred by averaging the parameter defined in Eq. (4) over the total number K of experiments:

$$\rho_{ij} := \frac{1}{K} \sum_{k=1}^{K} \rho_{ij,k} \tag{5}$$

Step 5. Data Processing Inequality (DPI): the interactions ρ_{ij} among all triplets of connected nodes are checked, and on the basis of their intensity one of them is possibly regarded as a false connection [38]. Suppose to have, for instance, three connected nodes w, y and z: if the influence ρ_{zw} that w has on z is lower than both the one that w has on y, that is ρ_{yw}, and the one that y has on z, that is ρ_{zy}, then the link between the pair (w, z) is removed, that is ρ_{zw} is set to 0. In particular, in order not to remove links in triplets that could actually be connected in the original topology, a further condition is added to the standard DPI, according to which false positives ρ_{ij} are removed as long as their value is below a certain threshold ν, with $0 \leq \nu < 1$ (Fig. 1). The higher the value of ν, the less connected triplets are found in the network.

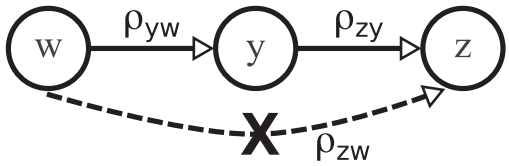

Figure 1: Data Processing Inequality. An edge going out of node i and coming in node j, where the direction is given by the arrow, is representative of the fact that node j is influenced by node i. Parameter ρ_{zw} is set to 0 as long as the three following conditions are verified simultaneously: 1) $\rho_{zw} < \rho_{yw}$, 2) $\rho_{zw} < \rho_{zy}$, 3) $\rho_{zw} < \nu$, where ν is a threshold value.

Step 6. Network Thresholding: all parameters ρ_{ij} whose value is below a certain threshold μ are set to 0, with $0 \leq \mu \leq \nu$ (the higher the value of μ, the sparser is the reconstructed network structure).

In order to investigate how the topology of the interactions among the nodes evolves over time, the time interval $[0, T]$ can be partitioned in L time windows $[t_l, t_{l+1}]$ of length ΔT_l, with $l = 0, \ldots, L-1$. REDRAW can thus be applied to measurements available for each of the L time intervals, so that the corresponding network

structure can be associated with each of them. The choice of ΔT_l is dependent on the specific application of interest and can be selected heuristically by trial-and-error.

Standard metrics are used to assess the performance of REDRAW [39]: Positive Predicted Value (PPV), Accuracy Rate (ACC), True Positive Rate (TPR) and False Positive Rate (FPR). They are provided as percentages, so that a network topology is perfectly inferred when $PPV = ACC = TPR = 100\%$ and $FPR = 0\%$. Details on their definition are given in [40].

Notably, we provided an algorithm for a sensible choice of the values that the thresholds ν and μ should take to remove possible false positives from the interconnections inferred in *Step 4*. Specifically, such algorithm relates topologies of different size to corresponding ranges of thresholds that maximize the metrics here considered when reconstructing an unknown network of interest. In particular, this is an a-priori method whose input consists in the size n of the network to reconstruct and N random graphs (each made up of n nodes) following the Erdös-Rényi model [41, 42], and whose output is an acceptable range of values for ν and μ. In particular, the algorithm reconstructs the assigned random graphs for different values of ν and μ, each leading to different values of the performance metrics, respectively. Only pairs (ν,μ) giving rise to acceptable values for such metrics are provided as output and should then be selected to reconstruct unknown topologies of interest. For further details on the aforementioned algorithm see [40].

3 Results

A network of $n = 4$ nonuniform Kuramoto oscillators described by Eq. (1) was first considered. Four different topologies (assumed to be unknown), respectively represented in Figs. 2(a)-2(d), were investigated. For each topology, $K = 50$ experiments of duration $T = 30$s were numerically simulated. For each node, experiment and topology, the natural frequencies ω_i were randomly extracted from the interval $[1, 2]$ rad s^{-1}, and so were the initial conditions $\theta_i(0)$ from the interval $[-\pi, \pi]$, $i = 1, \ldots, 4$. The model parameters were set to $c = 10$ and $\phi = \frac{\pi}{4}$ so that phase-locking could be achieved, while the thresholds were set to $\nu = 0.9$ and $\mu = 0.8$ following the algorithm in [40].

The reconstructed networks are represented in Figs. 2(e)-2(g), respectively. For each topology, neither missing links nor false positives are found, and the directionality of the links is correctly inferred for all of them ($PPV = ACC = TPR = 100\%$, $FPR = 0\%$). As for the weights, their magnitudes' relative relationship in the assigned topologies is correctly inferred as well. For instance, note how $a_{34} < a_{23} < a_{12}$ in Fig. 2(b) corresponds to $\rho_{34} < \rho_{23} < \rho_{12}$ in Fig. 2(f), or how $a_{31} = a_{41} < a_{12}$ in Fig. 2(c) corresponds to $\rho_{31} = \rho_{41} < \rho_{12}$ in Fig. 2(g).

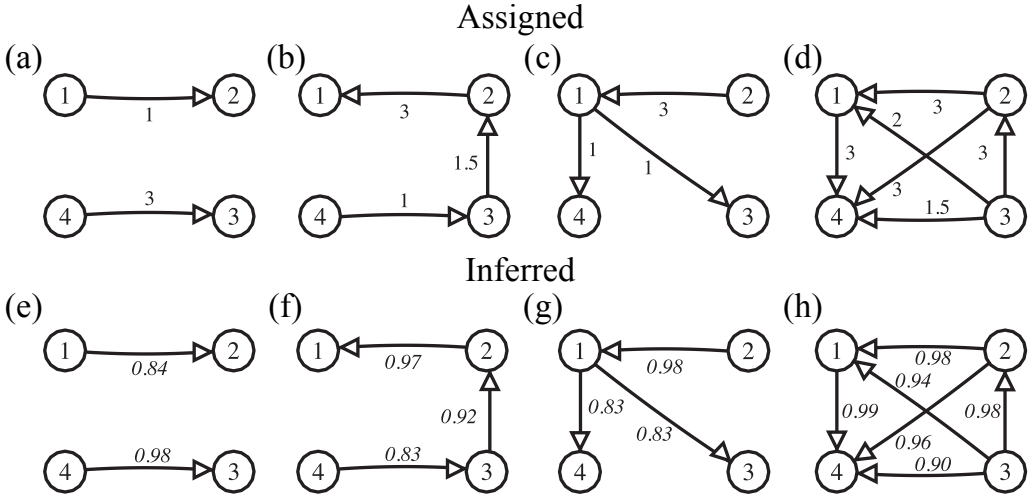

Figure 2: Assigned and inferred topologies, $n = 4$. The topologies on top (a-d) represent those used in the numerical simulations to generate the data-set then employed to obtain the inferred topologies, respectively represented in the bottom panels (e-h). The numerical values on the edges of the assigned topologies represent the values of a_{ij} in the model described in Eq. (1), whereas the italic numerical values on the edges of the inferred topologies represent parameters ρ_{ij} estimated by REDRAW.

The evolution over time of the reconstructed network with topology represented in Fig. 2(c) was inferred over time windows of length $\Delta T_l = \Delta T = 0.5$s, and it is shown in Fig. 3 (analogous results are found for the other topologies, data not shown). Notably, none of the nodes are connected before $t = 0.5$s, and then the stronger connection between nodes 1 and 2 is inferred before the others (the reconstructed topology does not change after $t = 3$s).

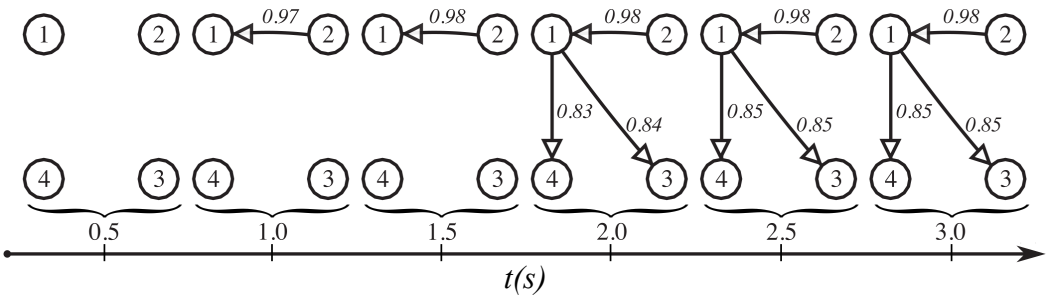

Figure 3: Topology of Fig. 2(c) inferred every 0.5s. The italic numerical values on the edges represent parameters ρ_{ij} estimated by REDRAW.

Next, we tested REDRAW on a larger network of $n = 17$ nodes. We generated data numerically by simulating the network over two different topologies (assumed to be unknown) with $c = 40$ so that phase-locking could be achieved, and set the threshold $\mu = 0.35$ while keeping all other parameters as in the previous example. The structures being considered were obtained by interconnecting four sub-networks with the structure represented in Fig. 2(d), either through a central hub in a *geometric graph* configuration [43] shown in Fig. 4(a), or as the *Ravasz-Barabási graph* [3] shown in Fig. 4(b), respectively.

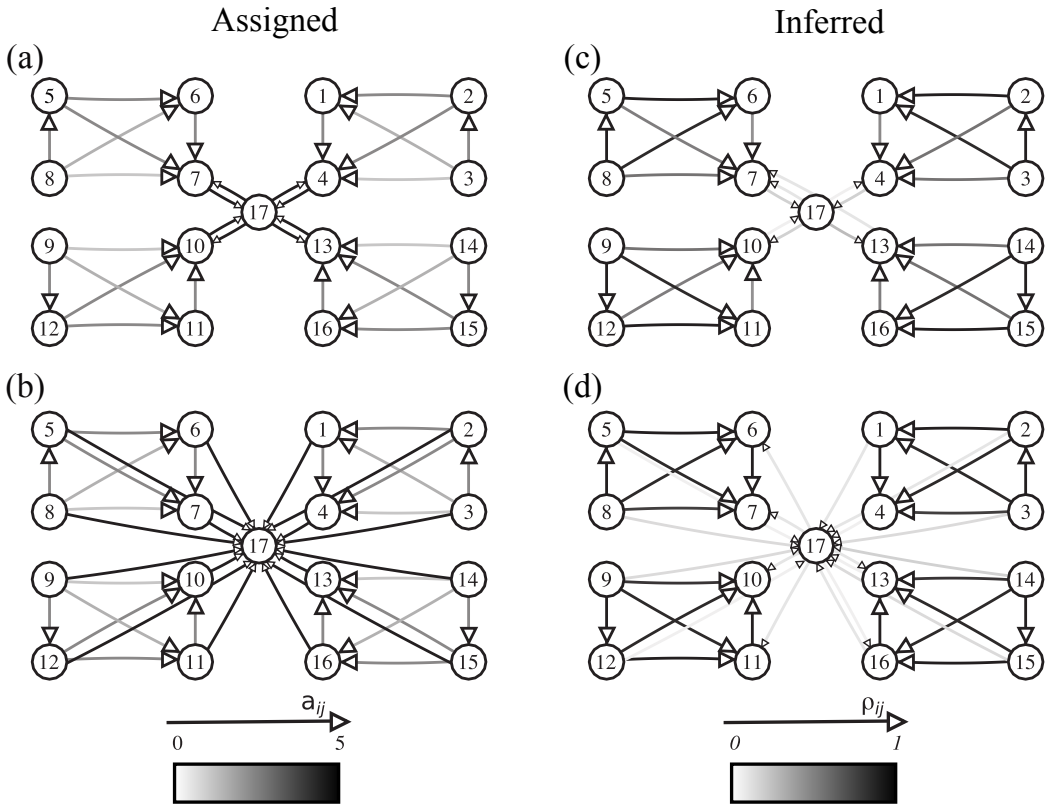

Figure 4: Assigned and inferred topologies, $n = 17$. The geometric graph (a) and the Ravasz-Barabási network (b) on the left-hand side represent the topologies used in the numerical simulations to generate the data-set then employed to obtain the inferred ones, respectively depicted on the right-hand side (c,d). Different scales of gray quantify the numerical value of a_{ij} for the assigned topologies, and ρ_{ij} estimated by REDRAW for the inferred ones.

The directionality of the geometric graph represented in Fig. 4(a) is correctly inferred for all its edges [Fig. 4(c)], with the only exception of a missing link from node 13 to node 17, replaced in the reconstructed topology by a link from node 13 to node 7. Although in the assigned topology the values a_{ij} of the edges within each sub-topology are lower than those connecting them to the central hub, the opposite result is found for ρ_{ij} in the inferred topology. This is due to the fact that the oscillators reach synchronization within each corresponding sub-group of four nodes (given the higher number of connections), hence exhibit greater phase mismatch with respect to the central hub.

Similar observations can be made for the Ravasz-Barabási network represented in Fig. 4(b). The direction-

ality is correctly inferred for all the edges belonging to each of the four sub-topologies, and for 12 out of the 16 edges connecting them to the central hub [Fig. 4(d)]. However, despite the values of a_{ij} in each sub-topology being lower than those related to the links connected to the central hub, the opposite result is found for ρ_{ij} in the inferred topology. This is due to the fact that, according to the assigned topology, the central hub is influenced by all the nodes in the network, hence its phase mismatch is minimized only with respect to an average value of the phases of all the other nodes.

We then applied REDRAW to reconstruct a network of $n = 20$ nodes. Data were obtained via numerical simulations carried out by considering the regular network structure shown in Fig. 5(a), and the structure obtained by some long-distance rewiring shown in Fig. 5(b), both assumed to be unknown. The coupling strength among nodes was set as $c = 50$ in the simulations so that phase locking could be achieved. REDRAW was parameterized by setting the thresholds to $\nu = 0.65$ and $\mu = 0.60$, following the algorithm in [40], with the other parameters being selected as before.

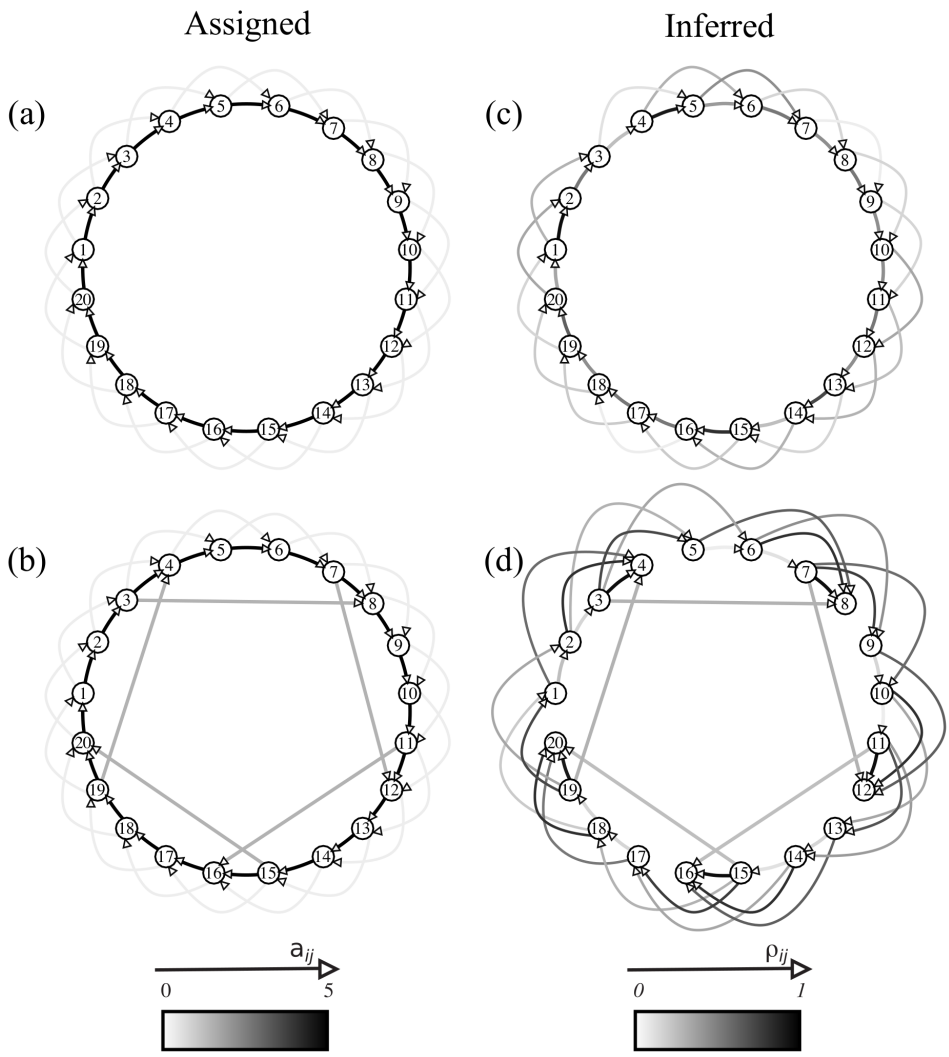

Figure 5: Assigned and inferred topologies, $n = 20$. The regular network (a) and that obtained by some long-distance rewiring (b) on the left-hand side represent the topologies used in the numerical simulations to generate the data-set then employed to obtain the inferred ones, respectively represented on the right-hand side (c,d). Different scales of gray quantify the numerical value of a_{ij} for the assigned topologies, and ρ_{ij} estimated by REDRAW for the inferred ones.

The directionality of the regular network represented in Fig. 5(a) is correctly inferred for all its edges [Fig. 5(c)], with the only exception of a missing link from node 2 to node 4. For each ith node, $i = 1, 2, \ldots, 20$, the edge coming from agent $i - 1$ has a higher inferred weight than that coming from agent $i - 2$ (note that agents $-1, 0$ correspond to agents $19, 20$, respectively), thus reproducing well the interactions assigned in the original topology.

The introduction of 5 edges [Fig. 5(b)] is well captured by the topology inferred in Fig. 5(d), leading to the formation of an equal number of clusters [nodes $(1 - 4)$, $(5 - 8)$, $(9 - 12)$, $(13 - 16)$ and $(17 - 20)$]. For each of the 5 nodes being influenced by one of the additional links (nodes $4, 8, 12, 16, 20$), no outgoing links are

Table 1: Metrics used to validate the effectiveness of REDRAW on networks of $n = 17$ and $n = 20$ nodes.

Topologies	**PPV**(%)	**ACC**(%)	**TPR**(%)	**FPR**(%)
Geometric graph	96.9	99.3	96.9	0.04
Ravasz-Barabási	86.4	97.1	95.0	2.60
Regular network	100	99.7	97.5	0
Rewired network	66.7	92.1	66.7	4.50

Table 2: Validation of REDRAW on the reconstruction of real-world networks. This table shows the four performance metrics (in percentages) obtained for each topology, together with their own number of nodes n and edges e, respectively. The values of coupling strength c and thresholds ν and μ employed in the numerical simulations are detailed as well.

Topologies	**n**	**e**	**c**	ν	μ	**PPV**	**ACC**	**TPR**	**FPR**
Enzyme-Catalyzed reaction pathway [30]	8	7	20	0.90	0.75	100	100	100	0
Songbird brain [31]	12	13	35	0.90	0.65	63	93	77	5
Bank stocks connections [32]	16	32	40	0.80	0.70	56	87	16	2
Human PPI [33]	23	22	40	0.80	0.50	100	98	45	0
Human PPI [33]	25	27	50	0.80	0.65	56	96	44	2
Hainan Power Grid Company [34]	48	63	150	0.60	0.60	52	97	62	2

inferred. This is a result of the model described in Eq. (1): for instance, the phase of node 4 is lowered by the influence of node 19, thus leading to higher mismatches of the former with nodes 5 and 6 (similar reasoning can be carried out for nodes 8, 12, 16 and 20).

Quantitative details on the effectiveness of the proposed method are given in Table 1 for the topologies represented in Figs. 4 and 5, respectively. In all the cases but for the network in Fig. 5(d), PPV, ACC and TPR take values close to 100%, while FPR takes values close or equal to 0%. In the remaining case, despite PPV and TPR taking values around 67%, the method still provides a low value of FPR (4.5%) and a high value of ACC (92.1%).

Finally, we used REDRAW to reconstruct some real-world networks existing in the current literature [30, 31, 32, 33, 34]. The values of the four metrics are detailed in Table 2 for different topologies characterized by a different number of nodes n and edges e, together with the value of the coupling strength c in the model described in Eq. (1), selected so that phase-locking could be achieved [37], and that of the thresholds ν and μ, selected as suggested by the proposed algorithm [40] – note how such thresholds converge towards each other as the number of nodes increases. All other parameters were kept as in the previous examples. The results in Table 2 confirm the effectiveness of REDRAW as method for reconstructing nonlinear heterogeneous oscillator networks. Indeed, for any of the considered real-world topologies, at least three out of four metrics take values representative of a correct inference.

For all the topologies considered in this work, we quantified the performance metrics for different numbers of experiments and observed how, for a sufficiently high number of repetitions, REDRAW is not sensitive to the specific value of K. For the sake of brevity, we here reported results only for the case $K = 50$; in fact, when $K \geq 50$, possible fluctuations of the metrics are negligible. For more details on the performance of REDRAW for different number of experiments see [44].

4 Conclusion and Discussion

We presented REDRAW as a network reconstruction method to infer directed and weighted links among groups of heterogeneous phase-locked nonlinear oscillators, whose interconnections were assumed to be unknown, and tested it in the particular case of networks of nonuniform Kuramoto oscillators for representative as well as real-world topologies. We observed how both directionality and weights could be correctly estimated with acceptable values of the performance metrics even in the case of larger networks.

Notably, we provided an algorithm for a sensible choice of the thresholds ν and μ employed to remove possible false positives from the inferred interconnections. Such algorithm is based on the reconstruction of random graphs following the Erdös-Rényi model [41, 42], and is presented in details in the accompanying supplementary material [40].

We plan on using REDRAW to infer the interactions underlying small-scale human ensembles engaged in multiplayer coordination tasks that require the group members to generate sinusoidal-like motions [45, 46, 47], and therefore give insights into their behavior when interacting together. Specifically, from the directionality of

the inferred links it is possible to detect the emerging leader in the group as the agent that influences the others the most in terms of highest number of outgoing edges [48], and hence decide what agent(s) could be possibly entrained (e.g., by an external audio/visual signal) for steering the whole group towards a desired behavior [49]. Moreover, from the weights of the inferred links it is possible to gain information on the partner(s) each participant prefers to interact with and on those s/he tends to avoid. This can offer a criterion to redefine the topology of the group interactions in order for each participant to maximize synchronization with all the others, which is fundamental when a high level of coordination is required in a human ensemble, as in music [50, 51] and sports [52, 53].

Acknowledgments

The authors wish to acknowledge support from the European Project AlterEgo FP7 ICT 2.9 – Cognitive Sciences and Robotics, Grant Number 600610.

References

[1] Strogatz SH. Exploring complex networks. Nature. 2001;410(6825):268–276.

[2] Albert R, Barabási AL. Statistical mechanics of complex networks. Rev Mod Phys. 2002;74(1):47.

[3] Ravasz E, Barabási AL. Hierarchical organization in complex networks. Phys Rev E. 2003;67(2):026112.

[4] Boccaletti S, Latora V, Moreno Y, Chavez M, Hwang DU. Complex networks: Structure and dynamics. Phys Rep. 2006;424(4):175–308.

[5] Buchanan M. Nexus: small worlds and the groundbreaking theory of networks. WW Norton & Company; 2003.

[6] Barabasi AL, Oltvai ZN. Network biology: understanding the cell's functional organization. Nat Rev Gen. 2004;5(2):101–113.

[7] Arenas A, Díaz-Guilera A, Kurths J, Moreno Y, Zhou C. Synchronization in complex networks. Phys Rep. 2008;469(3):93–153.

[8] Cardillo A, Petri G, Nicosia V, Sinatra R, Gómez-Gardeñes J, Latora V. Evolutionary dynamics of time-resolved social interactions. Phys Rev E. 2014;90(5):052825.

[9] Lungarella M, Pitti A, Kuniyoshi Y. Information transfer at multiple scales. Phys Rev E. 2007;76(5):056117.

[10] Liu YY, Slotine JJ, Barabási AL. Controllability of complex networks. Nature. 2011;473(7346):167–173.

[11] Menolascina F, Fiore G, Orabona E, De Stefano L, Ferry M, Hasty J, et al. In-vivo real-time control of protein expression from endogenous and synthetic gene networks. PLoS Comput Biol. 2014;10(5):e1003625.

[12] Kralemann B, Pikovsky A, Rosenblum M. Reconstructing phase dynamics of oscillator networks. Chaos. 2011;21(2):025104.

[13] Crampin E, Schnell S, McSharry P. Mathematical and computational techniques to deduce complex biochemical reaction mechanisms. Prog Biophys Mol Biol. 2004;86(1):77–112.

[14] Bansal M, Belcastro V, Ambesi-Impiombato A, di Bernardo D. How to infer gene networks from expression profiles. Mol Syst Biol. 2007;3(1):78.

[15] Barzel B, Barabási AL. Network link prediction by global silencing of indirect correlations. Nat Biotechnol. 2013;31(8):720–725.

[16] Sun J, Taylor D, Bollt EM. Causal network inference by optimal causation entropy. SIAM J Appl Dyn Syst. 2015;14(1):73–106.

[17] Bagrow JP, Bollt EM. Local method for detecting communities. Phys Rev E. 2005;72(4):046108.

[18] Sun J, Bollt EM. Causation entropy identifies indirect influences, dominance of neighbors and anticipatory couplings. Phys D. 2014;267:49–57.

[19] Villaverde AF, Banga JR. Reverse engineering and identification in systems biology: strategies, perspectives and challenges. J R Soc Interface. 2014;11(91):20130505.

[20] Staniek M, Lehnertz K. Symbolic transfer entropy. Phys Rev Lett. 2008;100(15):158101.

[21] Schreiber T. Measuring information transfer. Phys Rev Lett. 2000;85(2):461.

[22] De Smet R, Marchal K. Advantages and limitations of current network inference methods. Nature Rev Microb. 2010;8(10):717–729.

[23] Marbach D, Prill RJ, Schaffter T, Mattiussi C, Floreano D, Stolovitzky G. Revealing strengths and weaknesses of methods for gene network inference. Proc Nat Acad Sci USA. 2010;107(14):6286–6291.

[24] Yu D, Righero M, Kocarev L. Estimating topology of networks. Phys Rev Lett. 2006;97(18):188701.

[25] Arenas A, Díaz-Guilera A, Pérez-Vicente CJ. Synchronization reveals topological scales in complex networks. Phys Rev Lett. 2006;96(11):114102.

[26] Kuramoto Y. Chemical oscillations, waves, and turbulence. vol. 19. Springer Science & Business Media; 2012.

[27] Timme M. Revealing network connectivity from response dynamics. Phys Rev Lett. 2007;98(22):224101.

[28] Acebrón JA, Bonilla LL, Vicente CJP, Ritort F, Spigler R. The Kuramoto model: A simple paradigm for synchronization phenomena. Rev Mod Phys. 2005;77(1):137.

[29] Antonioni A, Cardillo A. Coevolution of synchronization and cooperation in networks of coupled oscillators. arXiv preprint arXiv:160703186. 2016.

[30] Villaverde AF, Ross J, Morán F, Banga JR. MIDER: network inference with mutual information distance and entropy reduction. PLoS One. 2014;9(5):e96732.

[31] Basso K, Margolin AA, Stolovitzky G, Klein U, Dalla-Favera R, Califano A. Reverse engineering of regulatory networks in human B cells. Nat Genet. 2005;37(4):382–390.

[32] Diebold FX, Yılmaz K. On the network topology of variance decompositions: Measuring the connectedness of financial firms. J Econometrics. 2014;182(1):119–134.

[33] Vinayagam A, Stelzl U, Foulle R, Plassmann S, Zenkner M, Timm J, et al. A directed protein interaction network for investigating intracellular signal transduction. Sci Signal. 2011;4(189):rs8–rs8.

[34] Chang L, Wu Z. Performance and reliability of electrical power grids under cascading failures. Int J Elec Power. 2011;33(8):1410–1419.

[35] Dorfler F, Bullo F. Synchronization and transient stability in power networks and nonuniform Kuramoto oscillators. SIAM J Control Optim. 2012;50(3):1616–1642.

[36] Zhang WY, Yang C, Guan ZH, Liu ZW, Chi M, Zheng GL. Bounded synchronization of coupled Kuramoto oscillators with phase lags via distributed impulsive control. Neurocomputing. 2016.

[37] See Supplementary Material for the definition of *phase-locking*.

[38] Margolin AA, Nemenman I, Basso K, Wiggins C, Stolovitzky G, Favera RD, et al. ARACNE: an algorithm for the reconstruction of gene regulatory networks in a mammalian cellular context. BMC Bioinformatics. 2006;7(Suppl 1):S7.

[39] DasGupta B, Liang J. Models and Algorithms for Biomolecules and Molecular Networks. John Wiley & Sons; 2016.

[40] See Supplementary Material for details on the algorithm employed for an optimal choice of thresholds ν and μ and for the definition of the standard metrics used to evaluate the performance of REDRAW.

[41] Erdös P, Rényi A. On random graphs, I. Publ Math Debrecen. 1959;6:290–297.

[42] Erdös P, Rényi A. On the evolution of random graphs. Publ Math Inst Hungar Acad Sci. 1960;5:17–61.

[43] Dall J, Christensen M. Random geometric graphs. Phys Rev E. 2002;66(1):016121.

[44] See Supplementary Material for detailed values of the standard metrics as a function of the number of experiments K.

[45] Alderisio F, Bardy BG, di Bernardo M. Entrainment and synchronization in networks of Rayleigh–van der Pol oscillators with diffusive and Haken–Kelso–Bunz couplings. Biol Cybern. 2016;110(2):151–169.

[46] Alderisio F, Fiore G, Salesse RN, Bardy BG, di Bernardo M. Interaction patterns and individual dynamics shape the way we move in synchrony. arXiv preprint arXiv:160702175. 2016.

[47] Alderisio F, Lombardi M, Fiore G, di Bernardo M. Study of movement coordination in human ensembles via a novel computer-based set-up. arXiv preprint arXiv:160804652. 2016.

[48] D'Ausilio A, Badino L, Li Y, Tokay S, Craighero L, Canto R, et al. Leadership in orchestra emerges from the causal relationships of movement kinematics. PLoS One. 2012;7(5):e35757.

[49] Wang Y, Doyle FJ. Exponential synchronization rate of Kuramoto oscillators in the presence of a pacemaker. IEEE Trans Autom Control. 2013;58(4):989–994.

[50] Badino L, D'Ausilio A, Glowinski D, Camurri A, Fadiga L. Sensorimotor communication in professional quartets. Neuropsychologia. 2014;55:98–104.

[51] Volpe G, D'Ausilio A, Badino L, Camurri A, Fadiga L. Measuring social interaction in music ensembles. Phil Trans R Soc B. 2016;371(1693):20150377.

[52] Wing AM, Woodburn C. The coordination and consistency of rowers in a racing eight. J Sports Sci. 1995;13(3):187–197.

[53] Silva P, Chung D, Carvalho T, Cardoso T, Davids K, Araújo D, et al. Practice effects on intra-team synergies in football teams. Hum Movement Sci. 2016;46:39–51.

SUPPLEMENTARY MATERIAL

Phase-locking

In order for REDRAW to correctly infer the structure of interconnections among n coupled oscillators, it is necessary for them to have achieved *phase-locking* as defined below.

Definition 1. *Denoting with $\theta_i(t),\ i = 1, ..., n$, the phase of the i-th oscillator in the network at time t, and with r and ψ the Kuramoto order parameters defined as:*

$$r(t)e^{j\psi(t)} := \frac{1}{n}\sum_{i=1}^{n} e^{j\theta_i(t)} \ , \tag{6}$$

we say that phase-locking *is achieved when*

$$c_v := \frac{\sigma}{\eta} \leq \chi \ , \tag{7}$$

where c_v, σ and η are coefficient of variation, standard deviation and mean over time of $\psi(t)\ \forall t \geq \hat{t}$, respectively, and $\chi > 0$ represents a certain upper bound.

As ψ represents the average angular velocity of all the oscillators, the previous condition guarantees that all their phase differences are bounded $\forall\ t \geq \hat{t}$.

Algorithm to select thresholds ν and μ

An important step in REDRAW when reconstructing the interactions among the nodes of a network whose topology is unknown, is the use of two filtering thresholds $0 \leq \nu < 1$ and $0 \leq \mu \leq \nu$: the former is used when applying *Data Processing Inequality* (DPI), the latter when removing some of the inferred links. The choice of such thresholds can be crucial, hence it is necessary to provide an *a-priori* criterion according to which acceptable values can be selected for them. Here we detail a possible algorithm to select the values of ν and μ (Figure 6).

Specifically, we suppose that a data-set is available for N different network configurations (assumed to be known) of n nodes reaching phase-locking, where n also corresponds to the size of the unknown topology of interest. For each of the N configurations, we assume K experiments are available, each of duration T. For each experiment, time-series for all the nodes are available. Then, we propose the following steps to select thresholds ν and μ that should eventually be employed when inferring the structure of interactions among the agents for which only experimental data is available (no a-priori information is given on their topology).

Step 1. Consider a two-dimensional grid made up of R points individuated by R respective pairs (ν, μ). Each of the N test-topologies is reconstructed by REDRAW for all the R threshold couples (ν, μ) such that $0 \leq \mu \leq \nu < 1$. As a result, RN topologies are inferred.

Step 2. For each of the RN reconstructed topologies, four standard metrics are computed. Specifically, the parameter ρ_{ij} inferred $\forall i, j$ through REDRAW is said to be a: True Positive (TP), if $\rho_{ij} > 0$ and $a_{ij} > 0$; False Positive (FP), if $\rho_{ij} > 0$ and $a_{ij} = 0$; True Negative (TN), if $\rho_{ij} = 0$ and $a_{ij} = 0$; False Negative (FN), if $\rho_{ij} = 0$ and $a_{ij} > 0$, where a_{ij} is the corresponding value in the topology originally assigned. Denoting with N_{TP}, N_{FP}, N_{TN}, N_{FN} and $N_{TOT} := n(n-1)$ the total number of true positives, false positives, true negatives, false negatives and possible links among all the nodes in the network, respectively, the performance metrics employed here are:

$$PPV := \frac{N_{TP}}{N_{TP} + N_{FP}},\ ACC := \frac{N_{TP} + N_{TN}}{N_{TOT}},\ TPR := \frac{N_{TP}}{N_{TP} + N_{FN}},\ FPR := \frac{N_{FP}}{N_{FP} + N_{TN}}.$$

Step 3. For each metric, acceptable bounds are defined according to the level of accuracy of the reconstruction that is desired. We term these bounds PPV^*, ACC^*, TPR^* and FPR^*. Averages of the RN values for each of the four metrics are computed across the N different structures. Thresholds ν and μ (i.e., the final output of the algorithm) are then selected so that the following conditions are simultaneously verified:

$$E[PPV] \geq PPV^*, \quad E[ACC] \geq ACC^*, \quad E[TPR] \geq TPR^*, \quad E[FPR] \leq FPR^* \tag{8}$$

where $E[M]$ denotes the average value of metric M.

In our work we take the following choices:

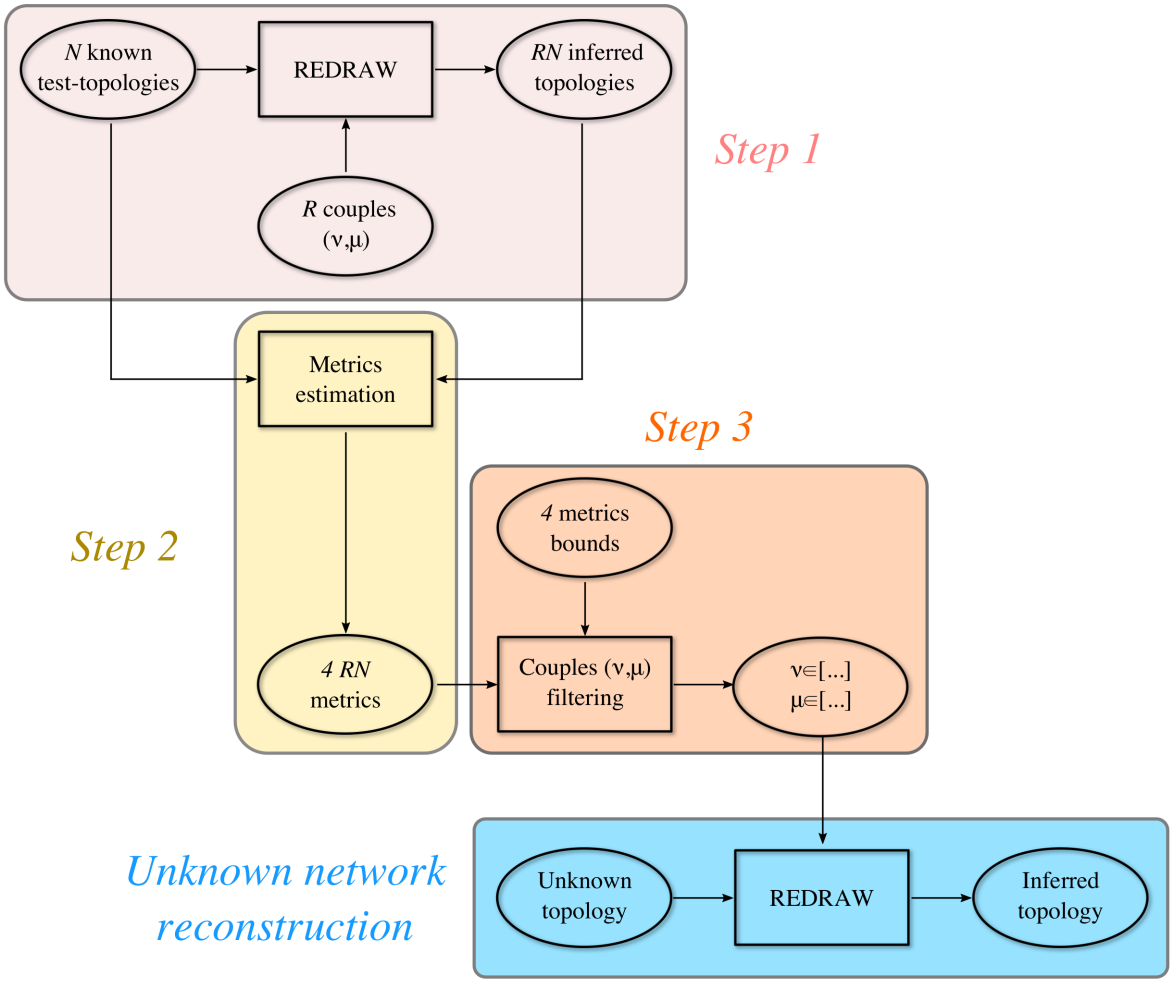

Figure 6: Algorithm to select acceptable threshold values for ν and μ. *Step 1*: N known test-topologies are reconstructed by REDRAW for R possible combinations of threshold couples (ν, μ). *Step 2*: for each of the RN reconstructed topologies, four standard metrics are evaluated. *Step 3*: averages of the RN values for each of the four metrics are evaluated across the N different structures, and thresholds ν and μ are selected so that four bound conditions are simultaneously verified. The thresholds thus obtained can then be selected to reconstruct an unknown topology of interest.

- We set $\chi = 35\%$, $\hat{t} = 20$s, $T = 30$s, $R = 5050$ (corresponding to sampling ν and μ in the interval [0,0.99] each with a step-size of 0.01), $N = 100$, $K = 10$, $a_{ij} = 1, 0$ according to whether node i is influenced by node j (there exists a link going from node j to node i) or not, respectively, $\phi = \frac{\pi}{4}$ and $c = 2.5n$ so that phase-locking could be achieved. For each node, experiment and test-topology, the initial conditions $\theta_i(0)$ are randomly extracted from the interval $[-\pi, \pi]$, and so are the oscillation frequencies ω_i from the interval $[1, 2]$ rad s^{-1}.

- We employ directed random graphs as test-topologies. Specifically, the Erdös-Rényi $G(n, p)$ model is used, where the probability p of a link connecting any two nodes in the network is independent on that of the others. We set such probability to $p = \frac{\ln n}{2n}$, which is likely to provide weakly connected graphs (their undirected version is connected).

- As the main goal is that of providing acceptable ranges within which ν and μ should take values for inferring unknown networks rather than known test-topologies, the metrics bounds for reconstruction of the latter need not be strict and can be chosen to be flexible. In particular, we set such bounds to PPV* =TPR* = 40%, ACC* = 70% and FPR* = 30%.

In what follows we illustrate the algorithm by using a collection of representative data-sets obtained by simulating $N = 100$ directed random graphs. We repeat the application of the algorithm to networks of different sizes to illustrate the effects of varying the number of nodes n in the network.

Test-topologies in *Step 1*

The second eigenvalue $\lambda_2(L)$ of the Laplacian matrix of the undirected version of the test-topologies, together with the respective coefficient of variation c_v obtained in the simulations, are detailed in Table 3.

Table 3: Values of $\lambda_2(L)$ and c_v averaged over the $N = 100$ directed random graphs employed as known test-topologies. For both measures, their value is represented for increasing number of nodes n, respectively.

n	5	10	15	20	25	30
$\lambda_2(L)$	0.86	0.46	0.43	037	0.40	0.51
$c_v(\%)$	1.3	4.3	7.6	8.4	11	10

***Step 2*: metrics evaluation**

The output of *Step 2* consists in $4RN$ metrics which can be depicted as heat maps, with different colors quantifying the value of the metrics. Specifically, dark (light) colors are representative of low (high) values (Figure 7). As the number of nodes n increases, PPV and TPR take lower values, whilst ACC and FPR do not vary as much.

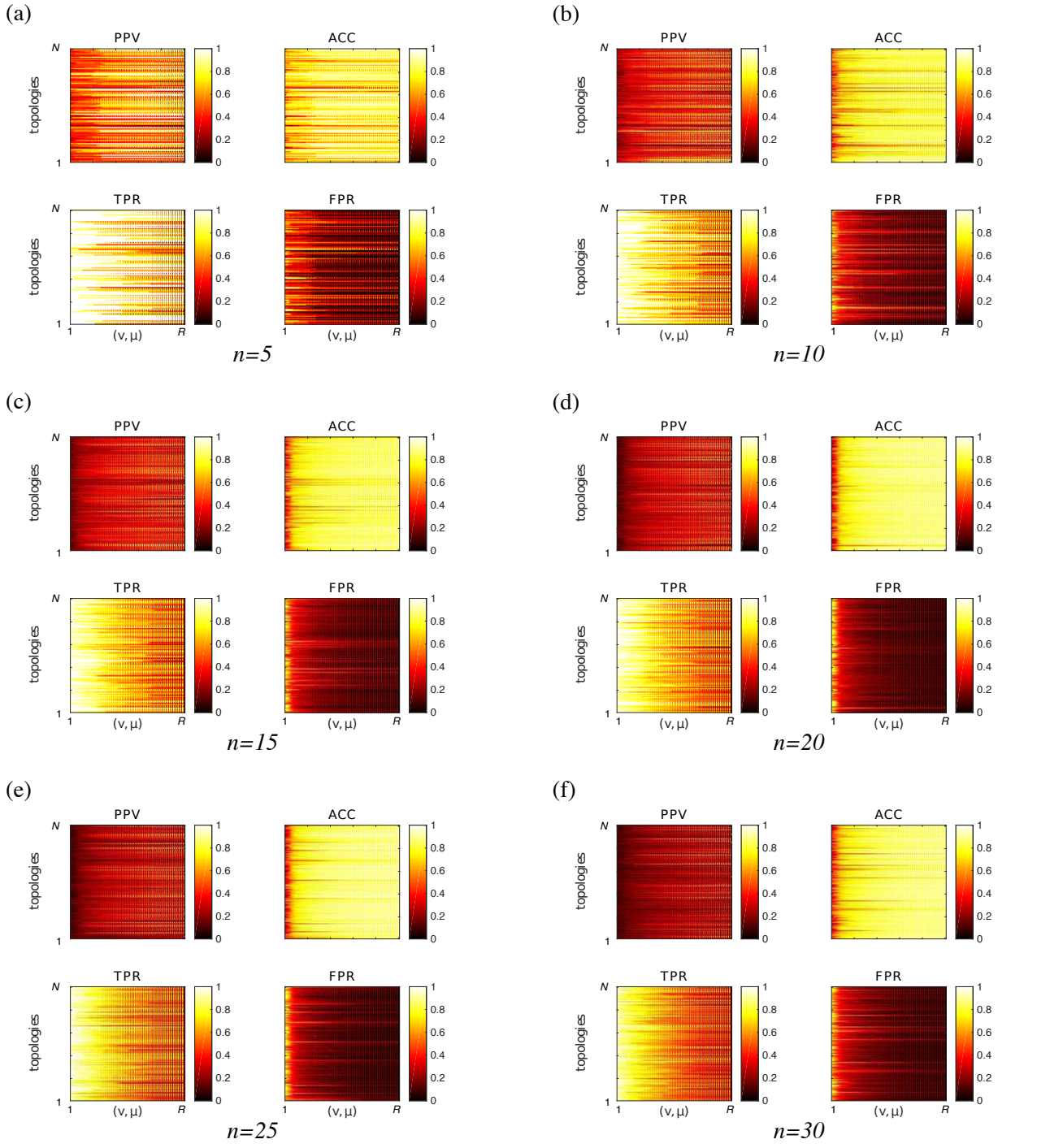

Figure 7: Output of *Step 2*. $4RN$ metrics, with $R = 5050$ and $N = 100$, are depicted as heat maps, where all the threshold couples $(\nu, \mu) \in [0, 0.99]^2$ are represented on the x axis, the topology index is represented on the y axis, and different colors quantify the value of the metrics, with dark (light) colors being representative of low (high) values. The results are shown for known test-topologies with a different number of nodes n. (a) $n = 5$, (b) $n = 10$, (c) $n = 15$, (d) $n = 20$, (e) $n = 25$, (f) $n = 30$.

Output of *Step 3*: acceptable values for thresholds ν and μ

The output of *Step 3* consists in acceptable ranges within which ν and μ should take values when reconstructing an unknown topology. It can be depicted as a shades-of-gray map (Figure 8), with lighter (darker) colors being representative of values for the threshold couples in correspondence to which more (less) metrics bounds conditions in Equation (8) are verified. Ideally, ν and μ should be chosen such that they individuate a point belonging to a white region (the bounds conditions are all simultaneously satisfied). If white regions are not found, a sensible choice would be to select threshold values that individuate points belonging to the lightest available region, or to relax the bounds conditions in Equation (8) and repeat the algorithm.

Note how, as the number of nodes n increases, the area of admissible regions where the threshold conditions in Equation (8) are all simultaneously satisfied shrinks (Figure 8).

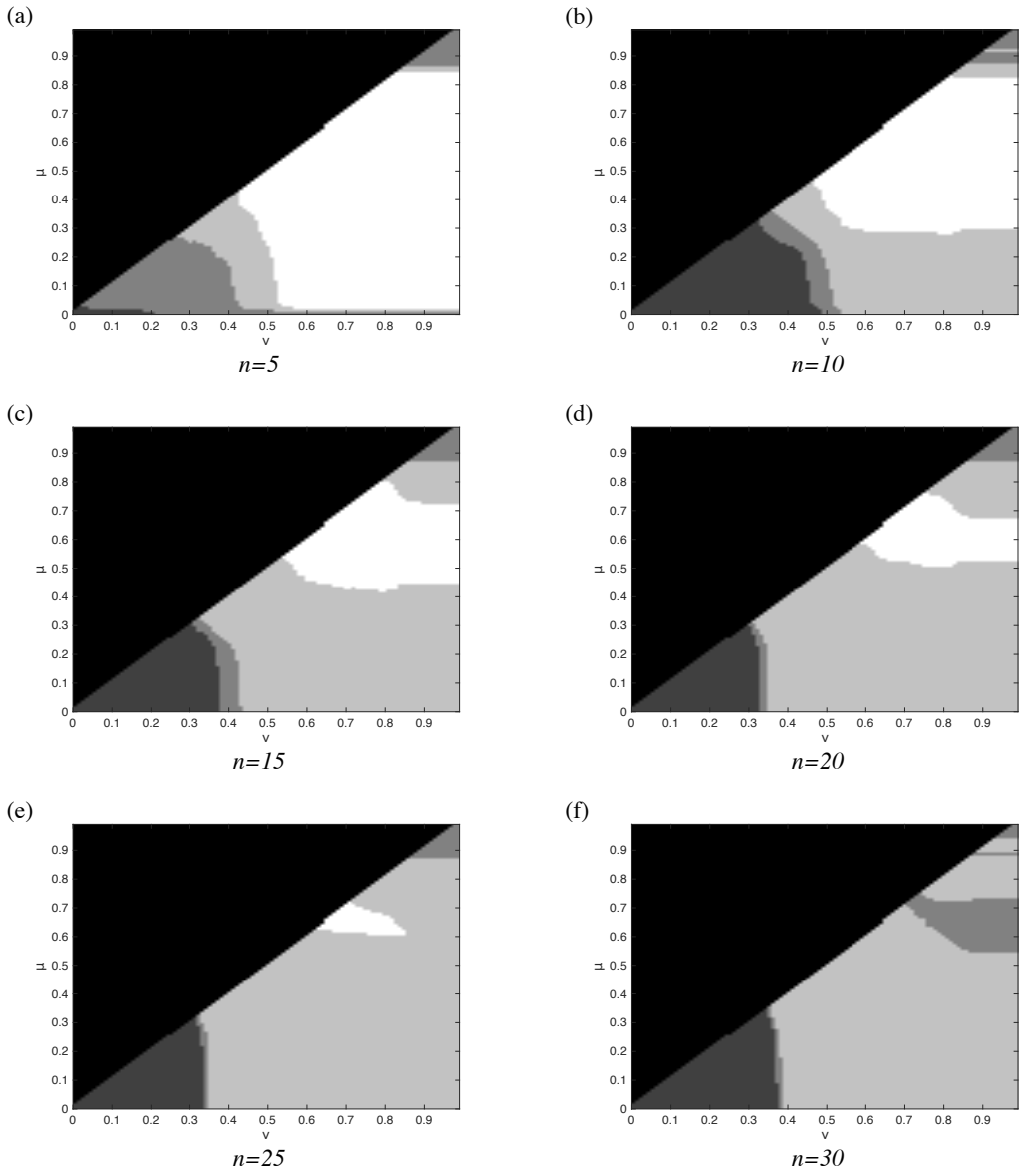

Figure 8: Output of *Step 3*. Acceptable ranges within which $\nu \in [0, 0.99]$ and $\mu \in [0, 0.99]$ should take values when reconstructing an unknown topology are depicted as a shades-of-gray map, where ν is represented on the x axis, μ on the y axis, and with lighter (darker) colors being representative of values for the threshold couples in correspondence to which more (less) metrics bounds conditions in Equation (8) are verified. White regions correspond to values of (ν, μ) for which the bounds conditions are all simultaneously satisfied. The results are shown for known test-topologies with a different number of nodes n. (a) $n = 5$, (b) $n = 10$, (c) $n = 15$, (d) $n = 20$, (e) $n = 25$, (f) $n = 30$.

Values of the metrics for different numbers of experiments

The four standard metrics are quantified in the main text for $K = 50$. In Figure 9 we show their values as a function of the number of experiments K employed to numerically generate the data-set. It is possible to appreciate how, for all the considered topologies, possible fluctuations of the metrics, due to the fact that each experiment is run with random values for both initial conditions and parameters of the nodes, are negligible when $K \geq 50$.

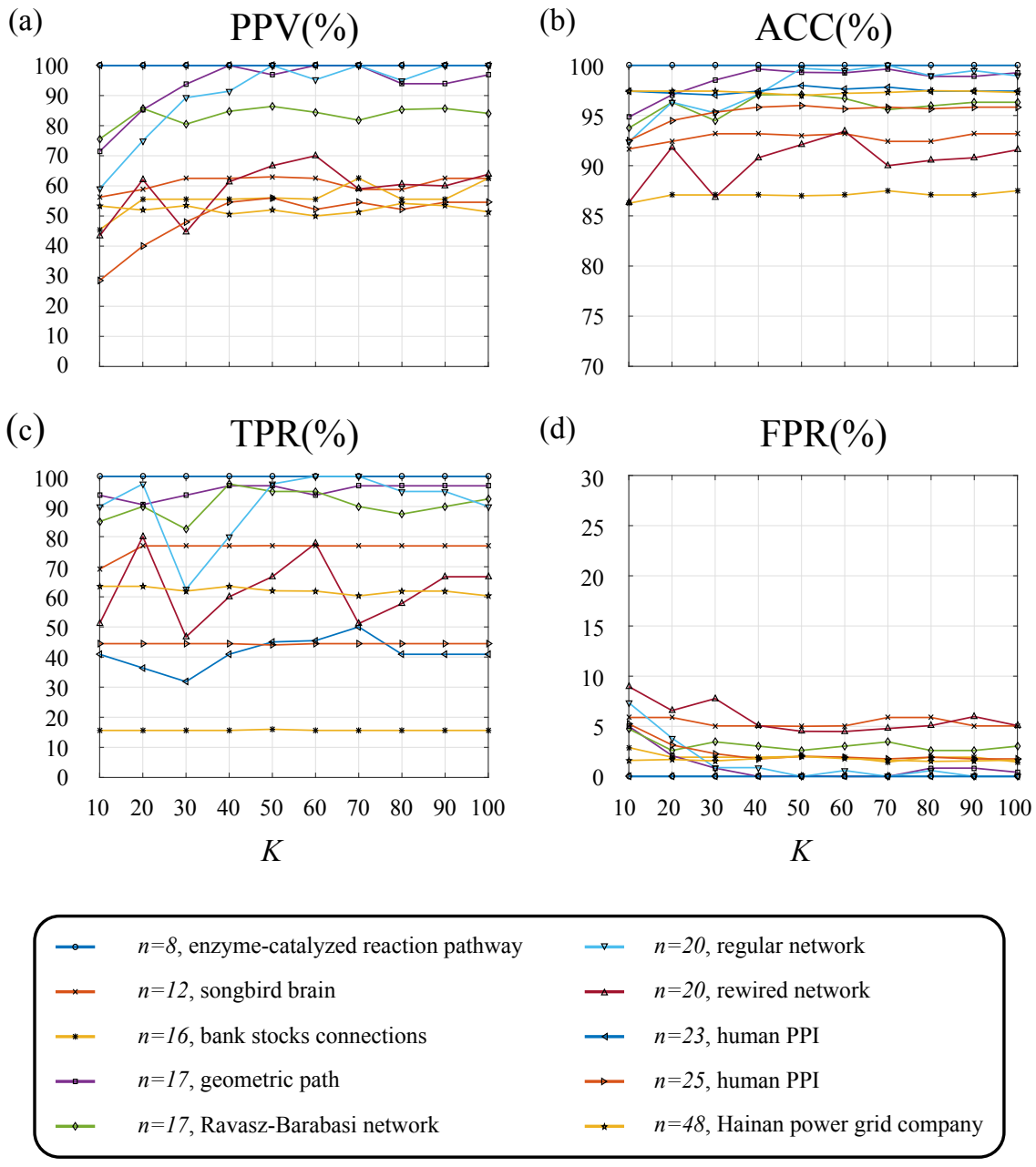

Figure 9: Values of the four metrics for different numbers of experiments K. Different colors and symbols refer to different topologies considered in the main text. (a) PPV: Positive Predictive Value, (b) ACC: Accuracy Rate, (c) TPR: True Positive Rate, (d) FPR: False Positive Rate.

For the sake of simplicity we do not show the value of the metrics for the *4-node* topologies considered in the main text: indeed, for these topologies the values of the metrics do not vary as the number of experiments K increases ($PPV = ACC = TPR = 100\%$, $FPR = 0\%$).